Nanoscale Advances

ROYAL SOCIETY OF CHEMISTRY

PAPER

View Article Online
View Journal | View Issue

Cite this: *Nanoscale Adv.*, 2020, **2**, 4951

Are TiO_2 nanoparticles safe for photocatalysis in aqueous media?†

Alexsandra Valério,[a] Marisa P. Sária,[b] Laura Rodriguez-Lorenzo,[b] Dachamir Hotza,[a] Begoña Espiña[b] and Sergio Yesid Gómez González *[a]

Received 16th July 2020
Accepted 14th September 2020

DOI: 10.1039/d0na00584c

rsc.li/nanoscale-advances

Although environmental and toxicity concerns are inherently linked, catalysis using photoactive nanoparticles and their hazardous potential are usually addressed independently. A toxicological assessment under the application framework is particularly important, given the pristine nanoparticles tend to change characteristics during several processes used to incorporate them into products. Herein, an efficient TiO_2-functionalized macroporous structure was developed using widely adopted immobilization procedures. The relationships between photocatalysis, catalyst release and associated potential environmental hazards were assessed using zebrafish embryonic development as a proxy. Immobilized nanoparticles demonstrated the safest approach to the environment, as the process eliminates remnant additives while preventing the release of nanoparticles. However, as acute sublethal effects were recorded in zebrafish embryos at different stages of development, a completely safe release of TiO_2 nanoparticles into the aquatic environment cannot be advocated.

Introduction

Titanium dioxide is the most commonly used nanomaterial worldwide; it is used as an ingredient in consumer products such as sunscreens, toothpastes, paints and papers, as well as in biological, environmental, and energy applications.[1] The production of TiO_2 nanoparticles is forecast at 2.5 million tons by 2025.[2] Nevertheless, this remarkable nanomaterial may exhibit potential adverse effects in natural systems.[3] This hazardous potential is routinely neglected in the photocatalysis in aqueous media.

More than half a century has passed since the beginning of water remediation using TiO_2 as the preferred photocatalyst.[4] As the leading semiconductor material for removing environmental pollutants, the mechanisms and disadvantages of TiO_2 have been systematically comprehended and addressed, leading to numerous enhanced TiO_2-based strategies for water splitting, wastewater treatment and related photocatalytic processes.[5–7] Largely studied and massively produced, TiO_2 is currently a key potential material for upcoming feasible industrial photocatalytic processes.

Photocatalysts in suspension are commonly used to demonstrate concepts in lab-scale research, mainly due to their simplicity. However, working with suspensions is not technologically feasible. Since the early 1980s, the concept of an immobilized photocatalyst on an inert support has been widely accepted to eliminate further costly separation processes.[8,9]

Immobilization is largely carried out *via* thermal treatment at low temperatures – from 50 °C to 300 °C – to prevent performance detriment and support degradation.[9–11] The quest for efficient photocatalysts and low-cost processes appear to have overshadowed concerns regarding the release of nanoparticles and their associated toxicity.

Furthermore, the toxicity assessment of TiO_2 nanoparticles has not kept pace with the rapid rise in their use, creating a knowledge vacuum.[12–14] Another challenge is the significant variability and uncertainty in data because after their manufacture, pristine nanoparticles are submitted to alterations *via* several processes that incorporate them into products.[15] Therefore, the toxicity profile must be considered under the product-application framework.

This study is aimed to determine the potential risks of TiO_2 nanoparticles in the context of aqueous photocatalysis. Here, a macroporous support functionalized with high-performance TiO_2 was developed by heat treatment. Tetracycline and carbamazepine were applied as model pollutants, and the discharge of nanoparticles was measured between degradation cycles. Subsequently, a complete *in vivo* assessment of the toxicity of the TiO_2 nanoparticles was carried out using the Acute Fish Embryo Toxicity (FET) test (OECD test guideline 236). Pristine, heat-treated and released nanotitania particles were tested among freshwater vertebrates to assess signs of toxicity and environmental risks associated with the developmental processes.

[a]*Department of Chemical and Food Engineering (EQA), Federal University of Santa Catarina (UFSC), 88010-970 Florianopolis, Brazil. E-mail: sergio.gomez@ufsc.br*

[b]*International Iberian Nanotechnology Laboratory (INL), 4715-330 Braga, Portugal*

† Electronic supplementary information (ESI) available: Statistical analysis of embryotoxic risk at different developmental traits and nanoparticles characterization. See DOI: 10.1039/d0na00584c

Results

Photocatalytic performance and particle discharge

TiO_2 nanoparticles were impregnated on PU sponge used as a support at 250 °C (HTS250 °C). Their tetracycline (TC) photocatalytic degradation over time was shown (Fig. 1A) to be approximately 100% after 120 min for a highly concentrated simulated effluent (10 mg L^{-1}). A similar trend was maintained at a lower tetracycline concentration. Reuse cycles were performed in a sequencing batch operation mode, analyzing up to 4 cycles; negligible differences in TC abatement were shown between the first and fourth cycles (Fig. 1B).

As seen for TC, photocatalysis of a highly concentrated carbamazepine (CBZ) solution with HTS250 °C (Fig. 1C) displays no significant variation between the first and fourth reuse cycles. Previously, it was demonstrated that a high CBZ concentration (10 mg L^{-1}) can be efficiently degraded by photocatalysis after 8 h under a 30 W UV-lamp using 100 mg L^{-1} of dispersed TiO_2 nanoparticles.[16] In this work, CBZ solution was treated at the solubility limit (20 mg L^{-1}) using 7 W, and more than 60% reduction of the pollutant was achieved in 180 min.

When the TiO_2 immobilization temperature was decreased to 100 °C (HTS100 °C), differences started to be reflected in the photocatalysis tests from the third cycle (Fig. 1D). To investigate the leakage profiles of the nanoparticles from the supports and their relationship with the photocatalytic performance, after each reuse run, the released nanoparticles were measured using inductively coupled plasma optical emission spectrometry (ICP-OES), as shown in Fig. 1E. Although HTS100 °C released ≈30% of the catalyst during the first remediation cycle, in the second cycle, it presented a slight improvement in the total CBZ abatement in comparison with its predecessor (Fig. 1F). Moreover, HTS250 °C showed unchanged CBZ profiles through time, notwithstanding the continuous TiO_2 release. The aforementioned results disclose that the discharge of particles can easily go unnoticed.

The supports of HTS100 °C and HTS250 °C were analyzed after the reuse cycles by X-ray photoelectron spectroscopy (XPS). XPS is a surface-sensitive technique that provides information about the changes in the chemical states of the coating particles and constituting species of the spent supports. Fig. 1G–I shows the high resolution XPS spectra for

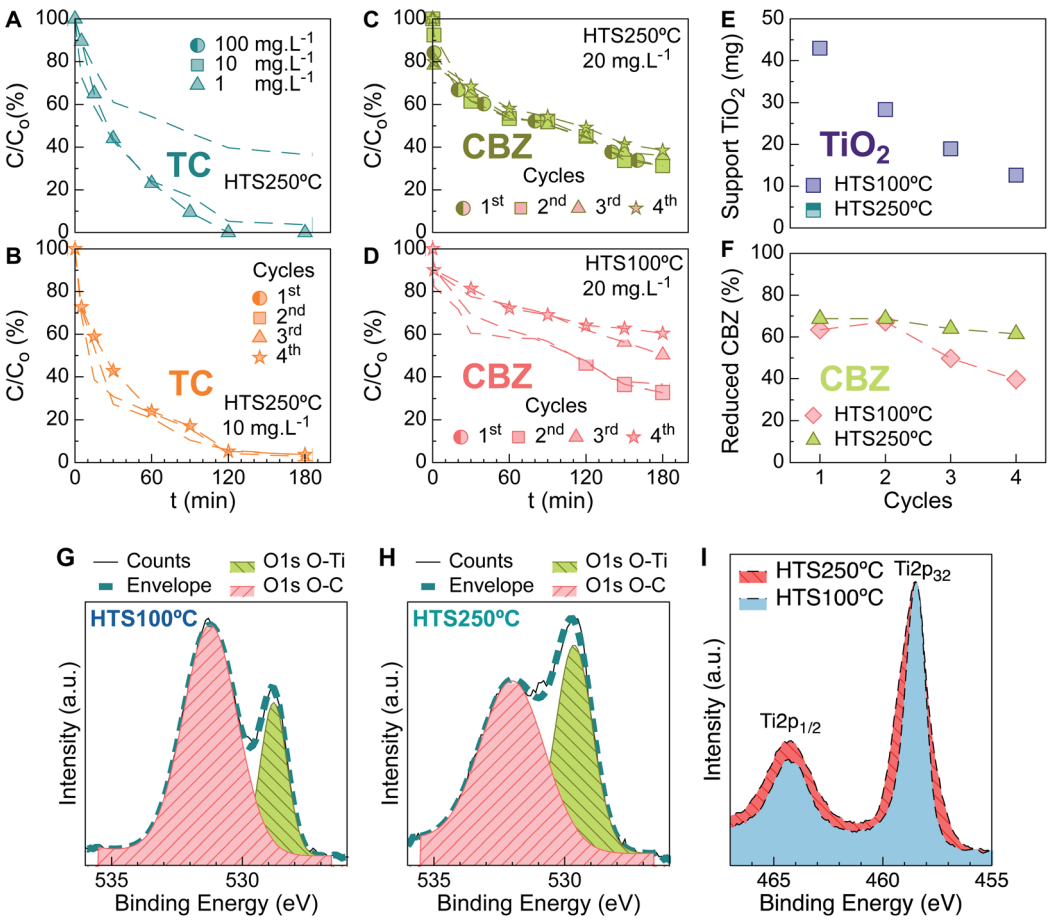

Fig. 1 (A) Photocatalysis of TC degradation using HTS250 °C ≠ initial concentration. (B) Photocatalysis of TC degradation with reused HTS250 °C, using 10 mg L^{-1} as the initial concentration. (C) Photocatalysis of CBZ degradation with reused HTS250 °C. (D) Photocatalysis of CBZ degradation with reused HTS100 °C. (E) Remaining supported TiO_2 nanoparticles at the beginning of each CBZ photocatalysis cycle. (F) CBZ abatement at the end of each cycle. Comparison of the high-resolution XPS spectra of the supports after the 4th cycle: (G) HTS100 °C O 1s, (H) HTS250 °C O 1s, and (I) Ti 2p HTS100 °C and HTS250 °C. TC = tetracycline, CBZ = carbamazepine, HTS100 °C = TiO_2 immobilized at 100 °C and HTS250 °C = TiO_2 immobilized at 250 °C.

both supports. In these spectra, the difference in the O 1s O–C and O–Ti components indicates a significant loss of TiO_2 particles for HTS100 °C, as measured by ICP-OES. The doublet Ti $2p_{3/2}$ (binding energy 458.6 eV) and Ti $2p_{1/2}$ (binding energy 464.4 eV) are consistent with Ti^{4+} in TiO_2, and the O 1s, O–Ti and Ti 2p components show wider lines (the full width at half maximum, FWHM, is 1.4 times wider). This indicates smaller TiO_2 nanoparticles on the support for HTS250 °C. This suggests that the photocatalysis performance is visibly affected immediately after releasing large amounts of finer catalyst particles. The comparative reuse profiles display accentuated efficiency loss, which indicates release of the nanoparticles from the support.

In vivo survival effects of the TiO_2 nanoparticles

The as-received TiO_2 nanoparticles showed significant lethality at the lowest and highest concentrations. This is mainly evident in later development, specifically at the eleuthero stage (Fig. 2A), correspondent to the start of dechorionated development (egg envelope absent, post-hatching) and transition to a lecitho-exotrophic larval phase.[17]

At the earliest hours of development, available data acknowledge a permeable trait of the chorion, the outermost membrane surrounding the embryo. This acellular envelope is pierced with structural pores and acts as a sieve, offering mechanical resistance to particles and limiting their internalization.[18] TiO_2 particles instantly aggregate in aqueous media (Table S2†), and a trend of increasing average size of the aggregates as the concentration increases has been discussed previously.[19] It is reasonable to presume that lower TiO_2 concentrations are more prone to easily trespass the chorion barrier. This barrier, in an early stage of development, surrounds an undifferentiated mass of embryonic cells that lacks organized multipart functional structures[17] and is thus unable to process the associated toxic effects. Therefore, a lag in increased acute toxic impairment at lower concentrations manifests itself until later development, as for 0.01 mg L^{-1} (Fig. 2A), because the first cells must still proliferate, differentiate, reorganize and connect to construct tissues and organs.

TiO_2 concentrations ranging from 0.1 to 10 mg L^{-1} correlate to higher survival rates at later stages. This is attributed to blocking of the large agglomerates at the chorionic pore channels. Indeed, the zeta potential (ZP) and dynamic light scattering (DLS) measurements indicate colloidal instability ($ZP = -6.47 \pm 0.50$ mV in freshwater) and a superior hydrodynamic average size in tank freshwater (Table S2†). The TiO_2 cluster is 30 fold larger ($\approx$630 nm) than the primary particle size ($\approx$20 nm) (Fig. 2D) and larger than the maximum diameter of the chorionic pore channels (around 400 nm at the inner layer[20]). This explains the absence of toxic signals at the eleuthero stage.

The same scenario can be equated to the highest concentration. In fact, larger agglomerates – (>1 μm) have been described for 100 mg L^{-1},[21] corroborating the findings at earlier development stages. However, a severe toxic trend was later observed (Fig. 2A), which is consistent with a correlative effect on the zebrafish embryo movements and breakage of the TiO_2 agglomerates with time. This constitutes a pragmatic rationale for dissimilar concentration-dependent trends later in development, as presented in the scheme in Fig. 2F. Agglomerate breakage and displacement of clumps can occur due to premature motion patterns, and related toxic levels can arise. Furthermore, at the eleuthero stage, dechorionated larvae are more vulnerable to prompt toxic risk. A mature neuronal framework is expected to command more responsive burst swimming, and orchestrated molecular trafficking with regulated metabolic routes manifests that permits rapid processing of the toxic outcomes.

Pristine nanoparticles were heat-treated to simulate the nanoparticles released from the HTS250 °C support. These nanoparticles showed less toxic development than those without thermal treatment (Fig. 2B and E). The similar hydrodynamic average sizes (Fig. 2D) and the recorded colloidal instability in the freshwater tank ($ZP = -1.12 \pm 0.51$ mV-Table S2†) explain the similar survival trends for the heat-treated and pristine nanoparticles. The divergence between the nanoparticles mentioned above is attributed to the size of the primary particles, which is slightly greater for heat-treated particles (Fig. 2D); this diminishes their overall reactivity and toxic potential, as discussed elsewhere.[22]

Prior to functionalization of the macroporous supports, Triton X-100 was used to disperse the TiO_2 nanoparticles. Despite their demonstrated capability of degrading biomembrane proteins and lipids,[23] causing severe impairment of cells and tissues through release of intracellular components, an irrelevant toxic effect was verified for the nanoparticles released from HTS250 °C (Fig. 2C), which even showed slightly lower toxicity than the heat-treated nanoparticles. Because the reused TiO_2 nanoparticles were heat-treated at 250 °C and immobilized on supports, Triton X-100 was eliminated, given that it is prone to degradation in air atmosphere above 200 °C.[24] In contrast, for the particles released from HTS100 °C (not shown), a total mortality of zebrafish embryos was registered. In fact, Triton X-100 leaching was undetected by using total organic carbon (TOC) measurements. However, the maximum tolerable concentration of this type of dispersant is remarkably low (0.01 wt%).[25]

In vivo sublethal effects of the TiO_2 nanoparticles

A general innocuous trend is attributed to the particles released from HTS250 °C during the reuse test, corresponding to the range of 1–10 mg L^{-1}, because several developmental traits did not reveal significant statistical differences from the control. In contrast, the pristine TiO_2 material caused effective toxic damage to different parameters (see ESI Table S1†). This effect is characterized by decreased spontaneous movements, increased heartbeat (Fig. 3A–C), and a downward trend of burst swimming. During phylotypic development, molecular facilitators of egg shell fracturing are secreted by gland cells,[26] triggering their softening and activating the abovementioned spinal-mediated coiled contractions towards hatching.[27] As normal extruding

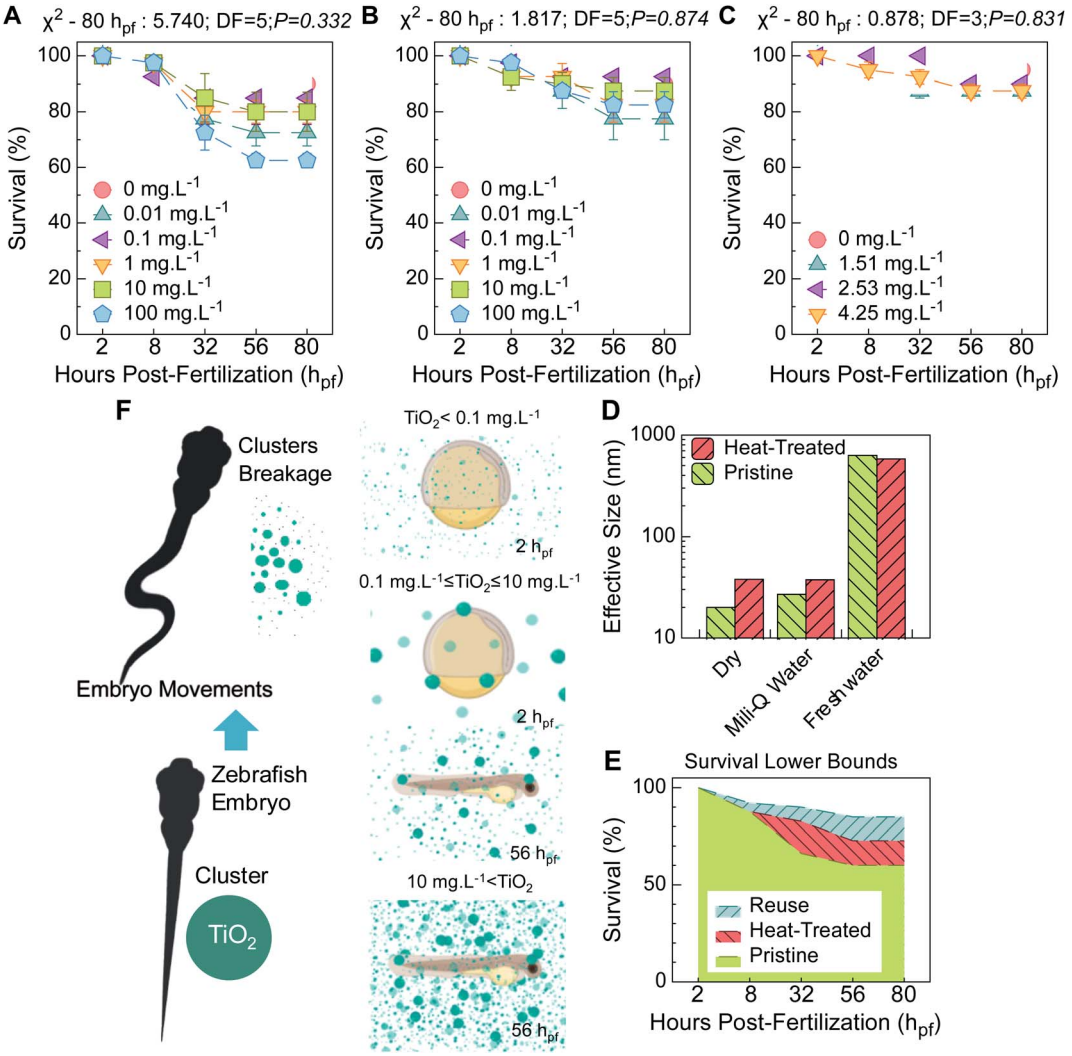

Fig. 2 Survival rates of zebrafish embryos exposed to TiO_2 nanoparticles: (A) pristine, (B) heat-treated, and (C) released during the reuse test for HTS250 °C. (D) Effective TiO_2 sizes (upper-right) for dry (transmission scanning microscopy, TEM), ultrapure water and tank freshwater (dynamic light scattering D_{50}, DLS). (E) Survival lower bounds (lower-right) for the data from (A), (B) and (C). (F) Scheme of the effects of toxicity on the movement of the embryos with concentration.

occurred (Table S1†), interference of TiO_2 in the hatching enzyme mollification task can be ruled out.[26] However, the pristine TiO_2 material seems to exert assertive toxic distress on zebrafish neurodevelopment at the eleuthero stage, affecting different *loci* that command neuromotor circuits at these traits;[26,28] this further substantiates the survival results (Fig. 2). For these parameters, thermo-treated TiO_2 revealed a less toxic trend than that from the reuse test; however, effects similar to those of the pristine TiO_2 material were minimized, showing a more expressive toxic risk only at the highest concentrations (Table S1†).

In the lecithotrophic period, zebrafish larvae act as a "sealed modulus" in terms of nutrient intake, remaining uninfluenced by external factors; therefore, their growth results from an exclusive reliance on the yolk sac. This trait is thus the most lipid-dependent and vulnerable to toxic risk in the first hours of development.[17] ANCOVA results on yolk (ball) volume did not attest significant interaction among groups for the pristine TiO_2 material, despite the fact that an increased trend was registered at approximately 1–10 mg L^{-1} (Fig. 3D). In the same range, thermal-treated TiO_2 did not reveal significant statistical differences from the control, but did at 100 mg L^{-1} (Fig. 3E). Moreover, for TiO_2 released during the reuse test, no statistical differences were found (Table S1†), although a downward trend can be noted (Fig. 3F).

Yolk lipids are known to decrease in absolute amount during development due to processing (at the yolk sac) prior to recruitment to the embryonic body.[28] As trunk straightening accompanies yolk extension formation, equating at some point to the greatest yolk ball diameter,[17] this decrease may be due to normal trafficking of lipids from the yolk to the organisms of developing larvae. At later stages, however, no relevant anomalous patterns were found in the yolk extension for the pristine nanoparticles. However, smaller pupil surfaces were measured (Table S1†). Because the most significant lipid depots are contained in the yolk and head (eyes and forebrain) of zebrafish

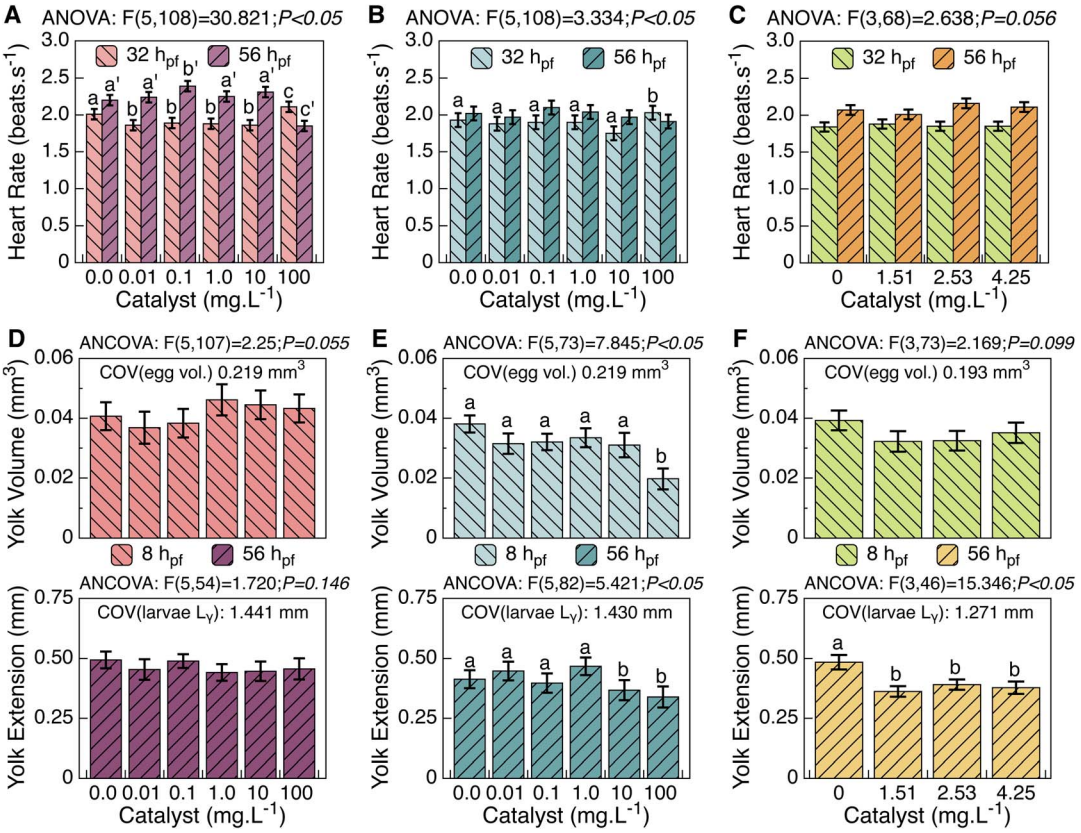

Fig. 3 Heartbeats of zebrafish embryos exposed to TiO_2 nanoparticles: (A) pristine, (B) heat-treated and (C) released during the reuse test. Effects on the yolks of zebrafish embryos exposed to TiO_2: (D) pristine material, (E) heat-treated nanoparticles and (F) released during the reuse test.

larvae,[29] these results may thus point to irregular lipid homeostasis *via* eventual interference of the pristine TiO_2 material in the energetic status of the zebrafish larvae. A trend of increased total body size was further measured (Table S1†), indicating plausible accelerated lipid transfer focused on larvae growth. Moreover, because decreased yolk volumes were found at advanced developmental stages, it can be suggested that the costs of this energetic process were supported through these earlier augmented lipid reserves.

Given that a higher probability of errors in normal embryonic development is expected in this substandard context, the structural defects were analyzed. Supporting these assumptions, yolk deformations, pericardial edemas, kinked notochords, arched tails and rhexis (vasculature shattering) were the most representative deviations observed. In agreement with the lethality results, the lowest and the highest TiO_2 concentrations correlated to higher numbers of occurrences of the mentioned defects (Fig. 4).

With regard to the thermo-treated TiO_2, the irregular trafficking of lipids anticipates a disruption in the energetic costs of embryogenic events, as increased pupil surfaces and decreased yolk volumes were measured during development (Table S1†). A remarkable decrease of yolk extension was observed at the highest concentration (Fig. 3B). Additionally, as ragged patterns were measured at the epibolic arc (Table S1†), lagged lipid metabolic processing at the yolk (ball) prior to transference to the embryonic body is reasonable. Moreover, higher head-trunk angles were registered at 100 mg L^{-1} (Table S1†), suggesting an accelerated event later in development. As previously mentioned, the pristine nanoparticles decreased spontaneous movements, and a downward trend for burst swimming was observed. Therefore, less affected by heat-treated particles, the embryo movements may increase the availability of smaller particles, increasing issues at latter stage. At 1–10 mg L^{-1}, the TiO_2 released upon reuse induced an effect on zebrafish yolk extension akin to that of thermo-treated TiO_2 (Fig. 3C). However, no unusual patterns were verified for the pupil surface, and no retarded developmental metrics were found for the epibolic arc or head-trunk angle (Table S1†). Additionally, fewer anomalies were observed in this TiO_2 range for the heat-treated nanoparticles (Fig. 4B). Only a statistical decrease of total body size was found (Table S1†). Because increased yolk volumes were found later in development, arrest of lipids at this stage can prevent regular energy transfer during the growth.

Discussion

The survival and sublethal tendencies observed in the photocatalytic essays confirmed that the proposed approach based on supported catalysts may enhance the applicability of photocatalysis in aqueous media. When the particles are supported

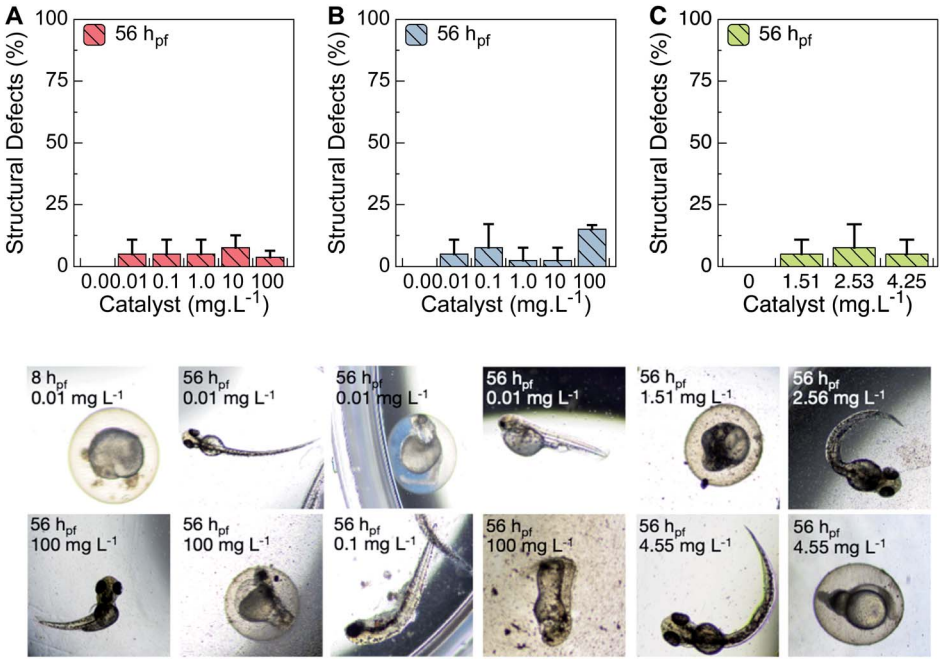

Fig. 4 TiO_2-induced structural defects in the developmental traits of zebrafish larvae, including representative anomalies registered below: (A) pristine nanoparticles, (B) heat-treated nanoparticles, and (C) particles released from HTS250 °C during the reuse test.

rather than dispersed in the effluent, burst particle release and remnant additives can be avoided when catalyst immobilization is used.

The macroporous support developed in this work is relatively simple to manufacture and highly efficient for the degradation of emergent pollutants. In this case, high amounts of pollutants were abated under mild conditions (40 mg L^{-1} TiO_2; 7 W UV-lamp). Furthermore, this support allows the use of improved hybrid processes such as photocatalytic ozonation.[30]

The release of particles is not straightforwardly related to remediation efficiency. In the present work, hindered efficiency was spotted immediately after 50% of the nanoparticles were lost when a large amount of smaller particles was discharged, according to XPS measurements. Therefore, during the development of new catalysts and the design of reactors, the release of particles should be verified through alternative techniques such as ICP-OES rather than correlating it with the efficiency rate.

As depicted in Fig. 3F, spread nanoparticles facilitate chorion penetration, triggering toxic effects at later stages. Moreover, mechanical breakage of TiO_2 clusters, caused by embryo movements, may lead to larger amounts of loose nanoparticles at later growth stages, increasing the toxicity effects. Taking a global perspective of the toxicological data, at 1–10 mg L^{-1}, corresponding to the frame test range in the catalyst release cycles using HTS250 °C, a superior clustering trend of thermo-treated nanoparticles was observed (Fig. 2D). The particles are prone to lipid–TiO_2 aggregate binding, which can affect trafficking of lipids at later stages of zebrafish development (Fig. 3D–F). The residual TiO_2 concentration as measured after the reuse tests may be a relevant indication to help choose the safest option for photocatalysis in an aqueous environment. Furthermore, previous studies showed that abiotic factors present under environmental conditions, such as humic acid and clays, reduce the toxicity of TiO_2 nanoparticles.[31,32] Those abiotic factors were not included in the tests here.

Another aspect to highlight is the adoption of a green synthesis process of the nanoparticles with the potential to reduce further acute effects reported here, as obtained with commercial TiO_2.[33,34] Additional care must be taken when using functionalized nanotitania because immunomodulatory effects by inducing inflammatory responses have been reported for those nanoparticles.[35]

Defected trafficking due to lipid arrest in the energetic reserve (egg yolk) can lag diffusion mobility and affect growth. TiO_2 released during reuse tests may result in a significant statistical decrease in the total body size of zebrafish larvae, in agreement with the former assumptions (Table S1†). In fact, steatosis effects on embryonic zebrafish exposed to TiO_2 were recently reported.[36] Irregular neutral lipid accumulation levels at the forebrain, notochord and tail of the larvae, coincident with the registered structural deformities (Fig. 4), were attributed to enhanced reactive conduct of TiO_2 with yolk syncytial layer apolipoproteins due to the increased zeta potential. Furthermore, the findings corroborate the size-dependent molecular interactions of TiO_2.

An occult deviation in protein expression levels as a consequence of TiO_2 exposure is also a rational premise that should not be ignored when interpreting effects on sublethal parameters flagging normal central nervous system development (Table S1†). An accentuated neurotoxic trend was verified for increasing concentrations of pristine TiO_2 material, which

causes sublethal effects on fundamental neuromotor embryonic traits (Fig. 3A–C). However, in the TiO_2 range tested for the catalyst reuse, these parameters were not affected as a consequence of exposure to thermal-treated nanoparticles or even to those released during the reuse assay (Table S1†). Thus, there is no amount of nanoparticles that can be released safely into the environment. However, acute sublethal effects were recorded less frequently for each condition tested, including serious structural defects not found in the control runs.

Experimental

Materials

Commercial TiO_2 nanopowder (P-25, Degussa), a non-porous 70 : 30 (w/w) mixture of anatase and rutile with a BET specific surface area of 55 ± 15 m^2 g^{-1}, was used as a photocatalyst. Tetracycline (TC, >99%, Meryer China) and carbamazepine (CBZ, >99%, Sigma-Aldrich) were employed as pollutants. Triton X-100 (Sigma-Aldrich) was used as a surfactant. Ultrapure water (Milipore, MiliQ) with a resistivity of 18.2 MΩ cm at 25 °C, pH 7.0 and TOC ≤ 5 μg L^{-1} was used for solution preparation and washing operations.

TiO_2-functionalized support preparation

Titania powder (40 mg) was supported on commercial highly porous (≈97%) polyurethane foams (PU, 20 ppi, FoamPartner, Switzerland). In order to assess the incorporation of TiO_2 on the surface of the macroporous support, two temperatures (100 °C and 250 °C) were evaluated for catalyst immobilization by thermal-induced fixation and to (totally or partially) remove the functionalization suspension precursors. For the support functionalization, TiO_2 nanoparticles were dispersed in 1 L of deionized water with the aid of a dispersant (5 wt%, Triton X 100, Sigma-Aldrich, Germany) to avoid particle agglomeration and precipitation. The TiO_2 suspension was kept in contact with the porous pristine PU cylindrically shaped support (700 mg; 5 cm diameter and 12 cm thickness) at room temperature for 1 h. After this time, the foam was dried for 12 h at room temperature. After drying, different supports were heated at 100 °C (S–TiO_2 100 °C) and 250 °C (S–TiO_2 250 °C) for 20 min in order to induce TiO_2 fixation on the macroporous structure and ensure surfactant removal.

Nanoparticles and support characterization

The size of the TiO_2 nanoparticles was assessed by transmission scanning microscopy (TEM, JEM-1011, 100 kV). Several drops of the diluted nanoparticles were placed on a carbon-coated copper grid, dried for 12 h and analyzed at 100 kV. The average diameter of the nanoparticles (ISO 22412:2017 particle size analysis) and the zeta-potential were measured by dynamic light scattering (DLS, 173°, Zetasizer Nano S, Malvern). Samples were prepared by dilution (1 : 10 in volume) in ultrapure water or tank freshwater, and the measurements were performed in triplicate ($n = 3$) at room temperature (25 °C). The total organic carbon (TOC) was measured by a TOC analyzer (Shimadzu-5050A). The samples were filtered through a Millipore-PVDF (0.45 mm) filter and directly analyzed. To analyze the surface characteristics, the spent supports were mounted on a sample holder with dimensions of 14 mm × 25 mm using adhesive double-sided carbon tape. X-ray photoelectron spectroscopy (XPS, ESCALAB250Xi, Thermo Fisher Scientific) was carried out with a hemispherical analyzer at an energy resolution of 0.1 eV with a field of view on the sample of ~0.9 mm. The X-ray source was monochromated Al Kα radiation ($h\nu = 1486.6$ eV), which was operated at 300 W and 15 kV. The diameter of the X-ray spot on the surface was 650 μm. The XPS spectra were collected at pass energies of 200 eV and 20 eV for the survey spectra and individual elements, respectively. A flood gun was used to compensate the surface charging during the XPS measurements. Argonium etching (Magcis, Thermo Fisher Scientific) was applied with an Ar ion source operated in monoatomic mode at 4 keV kinetic energy, a sputtered area of 2 × 2 mm^2, and a sputtering rate (calibrated for Ta_2O_5) of 0.55 nm s^{-1}.

Adsorption and photocatalytic degradation

TiO_2 supported on macroporous foams treated at 100 °C and 250 °C, named HTS100 °C and HTS250 °C, respectively, were used for the degradation experiments. For each run, the catalyst was placed inside the reactor around the quartz tube that protects the UV lamp by covering its entire length (12 cm). A solution was prepared by dissolving the pollutants (TC or CBZ) in 5 mL ethanol and then dissolving them in 995 mL of ultrapure water (Milipore, MiliQ). Afterwards, the solution in contact with the supported catalyst was subjected to artificial 7.0 W UV-light and magnetically stirred (100 rpm) for 30 min to reach the adsorption–desorption equilibrium. To assess the adsorption of titania nanoparticles on the support, an experimental study was carried out before each run in the dark for 60 min. Before the adsorption test, the UV-lamp was turned on and the solution was maintained for another 180 min under irradiation at room temperature. Aliquots were collected by pipetting 10 mL from the reaction broth to measure the CBZ concentration with a UV-Vis spectrophotometer (Lambda 950, PerkinElmer) at a wavelength of 200 to 400 nm.

Reuse cycles

TiO_2-functionalized supports were subjected to 4 reuse cycles under the same conditions as the initial aforementioned degradation test. After each cycle, the support was gently washed 3 times with ultrapure water (Milipore, MiliQ), dried at room temperature for 12 h, and then used in a new cycle. Each new cycle was carried out with fresh pollutant solution. The released TiO_2 was measured by inductively coupled plasma optical emission spectrometry (ICP-OES 9000, Shimadzu). Briefly, samples collected after the release experiments were treated with a mixture of HNO_3 : H_2SO_4 v/v at 70 °C for 2 h and subsequently left at 350 °C until complete evaporation. The digested samples were collected, transferred to 15 mL Falcon tubes and diluted to 10 mL with acidic water (2 wt% HNO_3). The treated samples were then measured by ICP-OES at emission wavelengths of 334.941, 336.121, and 337.280 nm. A standard curve of the aqueous Ti solutions was recorded to quantify the amount of released TiO_2.

Zebrafish spawning and eggs assortment

Wild-type zebrafish adults were used as breeders. Animals were housed in a 50 L dechlorinated and aerated freshwater tank, coupled with unidirectional recirculation flow and containing mechanical and biological filters, at 25 ± 1 °C under controlled photoperiods (14 : 10 h light : dark). *Ad libitum* feeding was ensured daily with the commercial diet Tetramin (Tetra, Melle, Germany), supplemented with live *Artemia* spp nauplii. A male-biased sex ratio cluster of spawners was transferred to a 30 L dechlorinated and aerated freshwater cage at 28 ± 1 °C under the same photoperiod as the housing tank. A few marbles were distributed at the bottom of the net-covered cage to furnish an artificial substrate for sexual stimulation of the females, as they tend to rub their genital papilla for gamete release. The males were then alerted and impelled to spread their sperm over the gametes. Parental predation of eggs was evaded through the net mesh size. At light onset, zebrafish sexual rituals were triggered conducting to external fecundation. Viable zygotes were then separated from unfertilized eggs under a stereomicroscope, taking into account the characteristic optical transparency of the former. Several washes were performed to remove parental fecal residues and protozoa, as these can potentiate contamination and affect the survival of zebrafish embryos at later developmental stages. The tank freshwater used for the above-mentioned procedures was pre-heated and filtered *via* a Millipore Stericup-GP sterile vacuum system coupled with a 0.22 μm pore size polyethersulfone membrane. The zebrafish embryos used in the experiment were derived from the same spawn of eggs, with a fertilization rate higher than 90%.

Zebrafish embryotoxic tests

Embryotoxic effects on zebrafish development were determined according to OECD test guideline 236 for the pristine TiO_2 material (P-25, Degussa) incorporated on the macroporous surface of HTS250 °C, functionalized TiO_2 nanoparticles submitted to the highest temperature treatment for fixation, and TiO_2 released from the same support during the reuse test. Ten viable 16-cell stadium eggs per replicate were arbitrarily transferred to 24-well microplates and subjected to continuous waterborne exposure to serially diluted nominal concentrations of 0, 0.01, 0.1, 1, 10 and 100 mg L^{-1} TiO_2 for 80 h_{pf}. The released concentrations of the tested TiO_2 were determined *via* ICP-OES, *viz.* 1.51, 2.53 and 4.25 mg L^{-1}, as mentioned in the Reuse cycles subsection. Four replicates of each TiO_2 test concentration were assessed. Pre-filtered freshwater collected from the fish tank was defined as the experimental control (zero mg L^{-1} of TiO_2). In prior experiments, pH measurements were conducted to ensure correspondence to the most favorable range reported for zebrafish. To ensure the finest environment temperature, indirect ultrasonic dispersion (20 min at 80%, 120 W, 40 kHz frequency) of the TiO_2 test concentrations was performed. Each day, these were left to acclimate at 26 ± 1 °C before renewal, as recommended by OECD 2013. The microplates were exposed to the same photoperiod as the breeders. Well sanitation was secured *via* regular inspection. To circumvent cross-contamination, dead fish were promptly removed. An experiment was classified as valid for a zebrafish embryonic mortality percentage inferior to 25% of the experimental control. At 8, 32, 56 and 80 h_{pf}, zebrafish embryonic development was staged, as in Kimmel *et al.*[17] Characteristic elemental morphological, functional and behavioral transformations at the indicated h_{pf} were used to flag toxic signals. For instance, at 8 h_{pf}, the epibolic arc perimeter is circa 3/4 of a complete event for normal development; at 32 h_{pf}, the head-trunk angle corresponds to about 90 degrees; the heartbeat is (generally) 2.00 ± 0.20 beats per s for 32 h_{pf} and 2.48 ± 0.29 beats per s for 56 h_{pf} (unpublished data); at the larval stage (80 h_{pf}), burst swimming is a reflex of normal neuro-motor developmental dynamics. For heart function assessment, twenty zebrafish embryos per test concentration were randomly selected, and the number of heartbeats was counted for 10 s. In order to avoid bias, "blind" observations were conducted by a single person. Specific developmental features (chorion, yolk, eye, and pupil) for each h_{pf}, were photographed using a Nikon Eclipse Ts2 inverted microscope coupled with a Nikon DS-Fi3 camera and measured to the nearest micrometer using the UTHSCSA Image Tool (v3.00). Sublethal endpoints were further assessed: hatching dynamics, aberrant cellular masses, structural defects, inconsistent movements, lagged characteristics and anomalous growth. The survival rates were recorded for different h_{pf}. Most test variables considered were conserved among vertebrate development, with marked implications at determinant embryonic events.

Statistical processing

Prior to data analysis, normality and homogeneity of variances were ascertained *via* Shapiro–Wilk and Levene's tests, respectively. To investigate the effects of TiO_2 exposure on the hatching rate (56 h_{pf}) and cumulative survival (80 h_{pf}) of zebrafish embryos, chi-square tests were performed with the observed values for each test condition (h_{pf} were analyzed separately). The null hypothesis of "no differences among groups" was considered for the establishment of the expected values (average hatching rate or total survival of all treatment groups for a given h_{pf}). One-factor ANOVA (six levels: 0, 0.01, 0.1, 1, 10 and 100 mg L^{-1} of the pristine TiO_2 nanomaterial or heat-treated nanoparticles; four levels of 0, 1.51, 2.53 and 4.25 mg L^{-1} of TiO_2 released during the reuse test) was conducted to investigate the effects of TiO_2 on the epiboly (8 h_{pf}), spontaneous movements and head-trunk angle (32 h_{pf}), and burst swimming (80 h_{pf}) of the zebrafish embryos. Analysis of covariance (ANCOVA) was applied to avoid biases associated with covariates to assess the effects of TiO_2 on the zebrafish yolk volume at 8 h_{pf} (egg volume was used as a co-variable), pupil surface at 32 h_{pf} (eye surface was used as a co-variable), and yolk extension at 56 h_{pf} (total body length was used as a co-variable). In order to investigate the impact of TiO_2 exposure on zebrafish embryonic heart and function, factorial ANOVA was applied [two factors: TiO_2 concentration (six levels: 0, 0.01, 0.1, 1, 10 and 100 mg L^{-1} of pristine TiO_2 material or heat-treated nanoparticles; four levels: 0, 1.51, 2.53 and 4.25 mg L^{-1} of TiO_2 released during the reuse test), and developmental ages (two

levels: 32 and 56 h_{pf})]. The Student–Newman–Keuls (SNK) test was used to establish post hoc interactions. A *P* value of 0.05 was rated for significance testing. Analyses were performed using Statistica v.7 (StatSoft, US).

Ethical annotation

Tests conducted on zebrafish embryos were in agreement with Directive 86/609/EEC. This comprises current guidelines defined at the Council of Europe on Protection of Experimental Animals, setting the regulatory limit of exposure to zebrafish at the free-living stage, corresponding to the end of their embryonic development. As 80 h_{pf} was the endpoint considered, lawful ethical consent was not required.

Conclusions

Immobilization processes of titania nanoparticles should be carefully designed to avoid remnants of the surfactants commonly used to disperse nanoparticle suspensions, which can cause a remarkable increase in the overall toxicity of the nanoparticles in aqueous media. The profile of the released nanotitania particles is not directly related to the water remediation yield. Therefore, large amounts of nanoparticles can be discarded without losing pollution abatement efficiency, indicating that environmental risk control cannot be based solely on application after measurement of the effects. The use of immobilized nanoparticles is the safest approach to address environmental concerns, as this process eliminates remnant additives while preventing release of the nanoparticles. However, within the range tested, there is no totally safe concentration of TiO_2 that can be released without potential hazard to the environment, as acute sublethal effects, even with lower frequency, were registered for all conditions. Therefore, more attention should be given to the release of nanoparticles in the design of immobilized reactors, as this issue is routinely neglected in photocatalytic technologies.

Author's contributions

A. V., M. P. S. and S. Y. G. G. wrote the first draft. A. V. performed all the experiments. M. P. S. supported and analysed the zebrafish toxicity experiments. A. V. and M. P. S. contributed equally to this work. L. R.-L supported and analysed the ICP-OES and photocatalytic measurements. S. Y. G. G. plotted and draw the figures. D. H., B. E. and S. Y. G. G. proposed the main ideas and supervised the data analysis. All the authors critically commented on and revised the manuscript.

Conflicts of interest

There are no conflicts to declare.

Acknowledgements

This study was supported by the International Iberian Nanotechnology Laboratory (INL) and Brazilian Center of Research in Physics (CBPF). L. R.-L. acknowledges the financial support from the EU Framework Programme for Research and Innovation H2020 COFUND, Grant Agreement 713640. M. P. S. and B. E. acknowledge the financial support from NanoDesk project (SOE1/P1/E0215) co-financed by the Interreg SUDOE Programme through the European Regional Development Fund (ERDF). A. V. D. H. and S. Y. G. G. are grateful for the financial support from Brazilian agencies CNPq and CAPES-PrInt (project number 88887.310560/2018-00).

Notes and references

1 W. A. Abbas, I. H. Abdullah, B. A. Ali, N. Ahmed, A. M. Mohamed, M. Y. Rezk, N. Ismail, M. A. Mohamed and N. K. Allam, *Nanoscale Adv.*, 2019, **1**, 2801–2816.
2 C. O. Robichaud, A. E. Uyar, M. R. Darby, L. G. Zucker and M. R. Wiesner, *Environ. Sci. Technol.*, 2009, **43**, 4227–4233.
3 M. Bundschuh, J. Filser, S. Lüderwald, M. S. McKee, G. Metreveli, G. E. Schaumann, R. Schulz and S. Wagner, *Environ. Sci. Eur.*, 2018, **30**, 6.
4 S. Horikoshi and N. Serpone, *Catal. Today*, 2020, **340**, 334–346.
5 J. Chen, F. Qiu, W. Xu, S. Cao and H. Zhu, *Appl. Catal., A*, 2015, **495**, 131–140.
6 S. Sun, X. Yu, Q. Yang, Z. Yang and S. Liang, *Nanoscale Adv.*, 2019, **1**, 34–63.
7 V. S. Sivasankarapillai, A. V. Kirthi, M. Akksadha, S. Indu, U. D. Dharshini, J. Pushpamalar and L. Karthik, *Nanoscale Adv.*, 2020, **2**, 1760–1773.
8 S. Suárez, in *Design of Advanced Photocatalytic Materials for Energy and Environmental Applications*, ed. J. M. Coronado, F. Fresno, M. D. Hernández-Alonso and R. Portela, Springer, London, 2013, pp. 245–267.
9 A. Y. Shan, T. I. M. Ghazi and S. A. Rashid, *Appl. Catal., A*, 2010, **389**, 1–8.
10 M. H. de Paiva Teixeira, L. A. Lourenço, W. Artifon, C. J. de Castro Vieira, S. Y. Gómez González and D. Hotza, *Fibers Polym.*, 2020, **21**, 90–102.
11 E. Adamek, W. Baran, J. Ziemiańska-Błaszczyk and A. Sobczak, *Sol. Energy*, 2019, **188**, 1232–1242.
12 W. N. Missaoui, R. D. Arnold and B. S. Cummings, *Chem.-Biol. Interact.*, 2018, **295**, 1–12.
13 R. Zhang, Y. Bai, B. Zhang, L. Chen and B. Yan, *J. Hazard. Mater.*, 2012, **211–212**, 404–413.
14 D. Minetto, G. Libralato and A. Volpi Ghirardini, *Environ. Int.*, 2014, **66**, 18–27.
15 A. R. Ribeiro, P. E. Leite, P. Falagan-Lotsch, F. Benetti, C. Micheletti, H. C. Budtz, N. R. Jacobsen, P. N. Lisboa-Filho, L. A. Rocha, D. Kühnel, D. Hristozov and J. M. Granjeiro, *NanoImpact*, 2017, **8**, 59–72.
16 H. Gulyas, M. K. Ogun, W. Meyer, M. Reich and R. Otterpohl, *Sci. Total Environ.*, 2016, **542**, 612–619.
17 C. B. Kimmel, W. W. Ballard, S. R. Kimmel, B. Ullmann and T. F. Schilling, *Dev. Dyn.*, 1995, **203**, 253–310.
18 D. Bonsignorio, L. Perego, L. D. Giacco and F. Cotelli, *Zygote*, 1996, **4**, 101–108.
19 O. Bar-Ilan, C. C. Chuang, D. J. Schwahn, S. Yang, S. Joshi, J. A. Pedersen, R. J. Hamers, R. E. Peterson and W. Heideman, *Environ. Sci. Technol.*, 2013, **47**, 4726–4733.

20 N. H. Hart and M. Donovan, *J. Exp. Zool.*, 1983, **227**, 277–296.
21 M. Faria, J. M. Navas, A. M. V. M. Soares and C. Barata, *Sci. Total Environ.*, 2014, **470–471**, 379–389.
22 N. S. Wigginton, K. L. Haus and M. F. H. Jr, *J. Environ. Monit.*, 2007, **9**, 1306–1316.
23 A. Pizzirusso, A. D. Nicola, G. J. A. Sevink, A. Correa, M. Cascella, T. Kawakatsu, M. Rocco, Y. Zhao, M. Celino and G. Milano, *Phys. Chem. Chem. Phys.*, 2017, **19**, 29780–29794.
24 J. A. Rojas, L. A. Ardila-Rodríguez, M. F. Diniz, M. Gonçalves, B. Ribeiro and M. C. Rezende, *Mater. Des.*, 2019, **166**, 107612.
25 *Diffusion of small molecules into medaka embryos improved by electroporation|BMC Biotechnology|Full Text*, https://bmcbiotechnol.biomedcentral.com/articles/10.1186/1472-6750-13-53, accessed April 6, 2020.
26 L. A. Fuiman, Special considerations of fish eggs and larvae, *Fishery Science, The Unique Contributions of Early Life Stages*, ed. L. A. Fuiman and R. G. Werner, Blackwell Science, 2002.
27 A. Kinkhabwala, M. Riley, M. Koyama, J. Monen, C. Satou, Y. Kimura, S. Higashijima and J. Fetcho, *Proc. Natl. Acad. Sci. U. S. A.*, 2011, **108**, 1164–1169.
28 D. Fraher, A. Sanigorski, N. A. Mellett, P. J. Meikle, A. J. Sinclair and Y. Gibert, *Cell Rep.*, 2016, **14**, 1317–1329.
29 V. Pirro, S. C. Guffey, M. S. Sepúlveda, C. T. Mahapatra, C. R. Ferreira, A. K. Jarmusch and R. G. Cooks, *Mol. BioSyst.*, 2016, **12**, 2069–2079.
30 A. Valério, J. Wang, S. Tong, A. A. Ulson de Souza, D. Hotza and S. Y. Gómez González, *Chem. Eng. Process.*, 2020, **149**, 107838.
31 K. Kansara, A. Kumar and A. S. Karakoti, *Sci. Total Environ.*, 2020, **698**, 134133.
32 G. S. Gupta, K. Kansara, H. Shah, R. Rathod, D. Valecha, S. Gogisetty, P. Joshi and A. Kumar, *Nanoscale Adv.*, 2019, **1**, 219–227.
33 M. Srinivasan, M. Venkatesan, V. Arumugam, G. Natesan, N. Saravanan, S. Murugesan, S. Ramachandran, R. Ayyasamy and A. Pugazhendhi, *Process Biochem.*, 2019, **80**, 197–202.
34 D. Hariharan, P. Thangamuniyandi, P. Selvakumar, U. Devan, A. Pugazhendhi, R. Vasantharaja and L. C. Nehru, *Process Biochem.*, 2019, **87**, 83–88.
35 V. Madhubala, A. Pugazhendhi and K. Thirunavukarasu, *Process Biochem.*, 2019, **86**, 186–195.
36 S. K. Verma, E. Jha, P. K. Panda, M. Mukherjee, A. Thirumurugan, H. Makkar, B. Das, S. K. S. Parashar and M. Suar, *Toxicol. Res.*, 2018, **7**, 244–257.